INTERNATIONAL JOURNAL OF INNOVATIVE RESEARCH & DEVELOPMENT

ISSN: 2278 – 0211 (Online)

Power Generation At Bulk Scale Operation Of Microbial Fuel Cell

Ankush Rai
CRIAD Laboratories, Smiriti Nagar, Chhattisgarh, India

Abstract:

Microbial fuel cells (MFCs) are an evolving technology for simultaneous bio-energy recovery and organic removal; however, the lack of studies conducted with large-scale MFCs, obstructs further development of this technology. This paper presents experimental result of Bulk-scale microbial fuel cell (BSMFC) operation where, we have built and operated a 4.9 L microbial fuel. BSMFCs so developed works on parallel stacked arrangement of brush anode with series cathode chamber which calibrates the maximum power delivery power up to 1.6 V across the load. However, except for the first phase of the whole experimental operation maximum power density is not maintained steadily. Its electricity generation & performance was examined. Moreover, we identified important issues for the failed attempt to continuously generate high power when MFCs are enlarged.

Key words: *microbial fuel cell; alternative energy; bioelectricity; large scale implementation.*

1.Introduction

It has been known for almost one hundred years that bacteria could generate electricity [1-3]. But only in the past few years this capability becomes more than a laboratory novelty. The MFC is a new form of renewable energy technology that can generate electricity from what would otherwise be considered waste. The reasons for this recent interest in using bacteria to generate electricity is the use of alternative energy resources that in the mean-time has already become a highly important issue in response to the current global energy crisis[4]. Direct bio-electricity production from organic compounds can be realized through microbial fuel cells [5-7]. The efficiency of this bio-electrochemical reactor depends a great deal on microbial metabolism while enabling these microorganisms to efficiently feed on organic compounds. The experimental results reported independently by teams of Delaney and Lithgow had exposed the metabolic pathway of microorganism-mediator-substrate combinations and selective bacterial mechanism of transport chain with hydrophilic redox mediators[8,9]. Many other parallel studies in subsequent years have triggered post-researches towards powering MFCs through Microbial Inoculants [10-12] & electricigens [13, 14]. Electricigens based MFCs employs Geobacter and Rhodoferax thus, marking a paradigm shift because these cells completely oxidize organic fuels while directly transferring electrons to electrodes without mediators.

Much understanding and progress have been achieved with the bench milliliter-scale (mL-scale) MFC reactors. Various bacterial strains have been tested in mL-scale MFCs and genetic studies helped reveal the mechanisms of electron transfer between bacterial cells and an electrode. 6 mL-scale MFCs also have been used to generate power from substrates in a wide range of complexity. Although microbial fuel cells are unlikely to produce enough electricity to contribute to the national power grid in the short-term, the cells may prove feasible in some specific instances such as covering the local energy needs for processing food wastes.

On the basis of previous studies on mL-scale MFCs most current research focuses on small-scale MFCs [24-27]. To make this technology practical requires critically investigating large-scale MFCs (litre-scale and beyond) and understanding the limitations that occur with the scale. This paper attempts to contribute to the current knowledge of litre-scale MFCs by studying a 4.9 L Bulk Scale Microbial fuel Cell, which is among the very few liter-scale MFCs reported in the literature. Examination of several operating parameters reveals the in depth calculation & simulated parameters for

implementing an effective large scale microbial fuel cell. Recent studies reported 0.6-0.7 V, consisting of single chambered MFC reactors, with a total volume of 3.5-4.0 L [15, 16]. By carefully controlling the catholyte pH and supply of pure oxygen, this 4.9 L BSMFC produced a maximum power density of 16W m^{-3}. In this study, we have mathematically modeled & simulated an operating Bulk Scale microbial fuel cell (BSMFC) with a volume of 4.9 L. We also examined the influence of membrane over the power generation. Our results provide information for an aid in full-scale MFC construction and operation.

This study is divided into 3 sections. In section 1, we examined our proposed design of Bulk-scale microbial fuel cell. Section 2, consists of modeling parameters & simulation for operating microbial fuel cell at large volume. Thirdly, Section 3 introduces an autonomous energy harvesting scheme that capture energy from BSMFC at the most efficient operating point and at the same time form the energy into a usable shape. Finally, we laid future prospect of this study on the basis of our investigation.

2.Reactor Setup

To date, the power density of MFCs is yet to reach a widely applicable level. The BSMFCs we have studied (see Figure.1.) has this multiple unit volume batch reactors where there is parallel stacked arrangement of brush anode with series cathode chamber, enlarging the electrode surface area, in order to increase MFC power capacity. In the scalable configurations electrodes were used as anodes, which were conductively connected to a brick or tubular-shaped membrane cathode. The maximum power density is generated by the MFC with inside-anode was twice that of the MFC due to a shorter electrode distance. Moreover, multiple brush anodes and cathodes are assembled in the same reactor to increase the reactor scale. Carbon fiber or carbon nano-tubular filaments were used as anode singly or to form an anode array. MFCs in the system are connected tail-to-head via insulating pipe. The anode was located inside the pipe, which was then wrapped with hot pressed membrane-cathode. In one embodiment, an MFC stack comprising 4 MFC units with wastewater pumped as medium. However, electrode separators are essential for an MFC stack, thus the best result was obtained by using pressed carbon paper as the separator. As mentioned the usage of layer of cation exchange membrane is omitted. However, this omission significantly decreased the MFC internal resistance [17,18]. For optimal operation, anode and cathode is kept close

together as possible [19]. Also proton migration significantly influences resistance-related losses [20]; adequate mixing had minimized these losses.

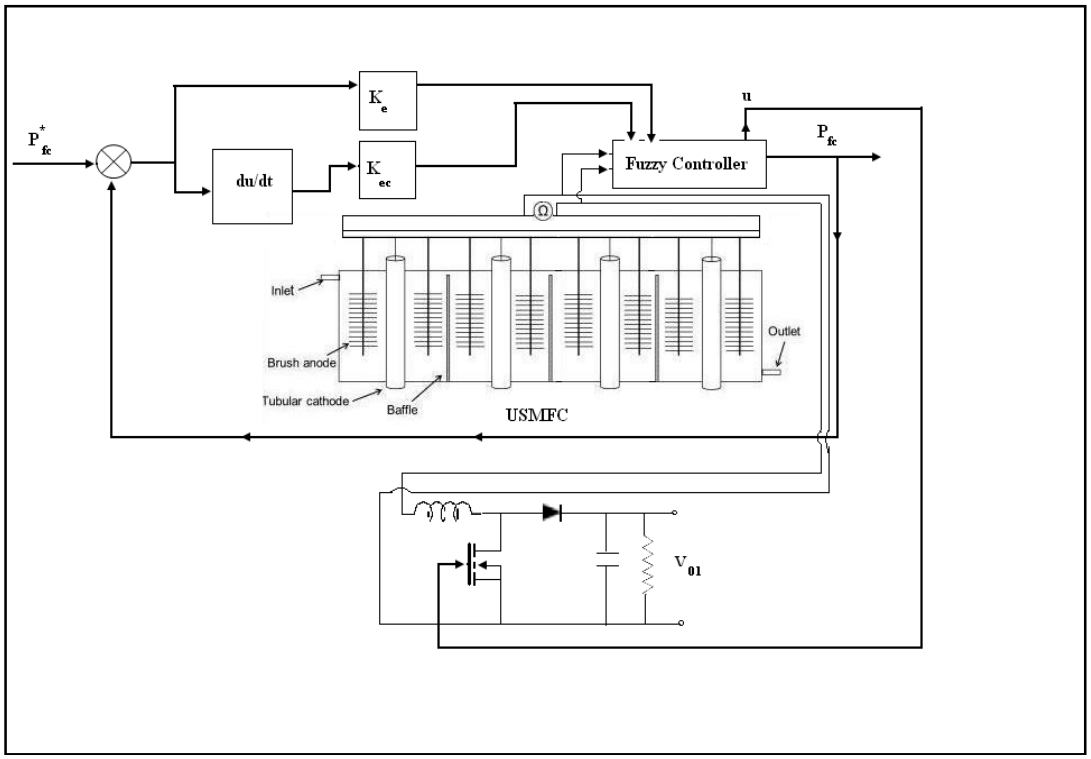

Figure 1: Schematic of BSMFC using brush anode & fuzzy logic energy harvester. Brush anodes are parallelly stacked together with series arrangement of cathode chamber

Nonlinear dynamics & the complexity of the fuel cell make the task difficult to maintain a fuel cell system in correct operating conditions. Fuzzy logic can capture the continuous nature of human decision processes and adds improvement over methods based on binary logic. Therefore, the fuzzy control system is used in this frame for maintaining the fuel cell system in correct operating conditions, to resist load disturbance & to obtain a constant power output. More details have been discussed in the subsequent sections.

Voltages are monitored every 3 min by a digital multimeter and a data acquisition system. Dissolved oxygen will be measured using a non-consumptive fiber optic oxygen probe and the manufacturer's software (OOIFOXY oxygen sensor software, v. 1.67.15F). Prior to measuring samples, the probe was calibrated with oxygen saturated medium (using air) in the same type of bottle, and medium in which the Dissolved Oxygen (DO) was scavenged using sodium hydrosulfite. Polarization curves were constructed using a Gamry Reference 600 potentiostat(Gamry

Instruments,Warminster,PA,USA)at a scan rate of 1 mVs^{1}. Power density, current density, and coulombic efficiency were calculated according to a previous study [21]. The pH was measured using a Benchtop pH meter(UB- 10, Denver Instrument, Denver, CO, USA).

S.No.	MFC Configuration	Maximum power or cuurent density	Reference
1	Single chamber MFC	18 W/m^3	22
2	Two chamber MFC	68.4 W/m^3	23
3	Cylindrical two chamber anode with a internal anode chamber	83 ± 11 W/m^3	24
4	Parallel stacked arrangement of brush anode with series cathode chamber	190 ± 5 W/m^3	Present study

Table 1: Comparison Of Configuration And Performance With Other Designs Of Microbial Fuel Cell

The BSMFCs we have studied (see Figure.1.) in the laboratory with this multiple unit volume batch reactors each stacked in series with brush anode enlarging the electrode surface area, in order to increase MFC power capacity. In the scalable configurations electrodes were used as anodes, which were conductively connected to a brick or tubular-shaped membrane cathode. The maximum power density is generated by the MFC with inside-anode was twice that of the MFC due to a shorter electrode distance. Moreover, multiple brush anodes and cathodes are assembled in the same reactor to increase the reactor scale. Carbon fiber or carbon nanotubular filaments were used as anode singly or to form an anode array.

3.BSMFC's Operational Condition

BSMFC consist of 3 x 4 graphite electrodes. Graphite electrode sized of > 280 cm^2 (10 X 2 cm) rectangular blocks was held co-planner in a plastic support. The distance between the two electrodes was 7 cm with all exposed metal surfaces sealed with the nonconductive epoxy. Electrodes were washed and soaked in double distilled water prior to use. The collected wastewater and sediment was transferred to the fish tank for the simulation of wastewater – sediment interface. After the formation of interface, BSMFC

was deployed in between the interface and allowed for settlement. Slowly the disturbed layer gets settled. The digital multimeter was connected to the BSMFC in open circuit in-order to observe the development of potential. The autoclaved sediment was used as control. BSMFC was operated in a constant room temperature (32 ± 2°C). The surface wastewater at cathode was sparged with air using an air pump. After the development of stable potential, power output was monitored by measuring voltage across an external resistance connected across the anode and cathode.

4.Electrochemical Analysis

4.1.Electrochemical Characteristics of BSMFC: Mathematical Modeling

The concentration of enzyme e is divided into three classes: enzyme's initial concentration be i_e, operating concentration of enzyme denoted as u_e and loitered concentration bev_e. Similarly, the substrate concentration S is divided into two classes: initial i_s and operating concentration of substrate denoted as u_s. By considering the criss-cross interaction of the concentration of substrate with the concentration of enzyme, the equations that describe the spread of the reaction can be written as:

$$\left.\begin{aligned}
\frac{di_e}{dt} &= \mu_e + A - k_{+1}i_e - c(S)i_e u_s + \delta v_e \\
\frac{du_e}{dt} &= c(S)i_e u_s - \gamma u_e - k_{+1}u_e \\
\frac{dv_e}{dt} &= k_{-1}(u_e) - k_{+1}v_e - \delta v_e \\
\frac{de}{dt} &= \mu_e + A - k_{+1}e \\
\frac{di_s}{dt} &= \mu_s - k_{-1}i_s - \beta_2 i_s u_e - \beta_3 i_s v_e \\
\frac{du_s}{dt} &= -k_{-1}u_s + \beta_2 i_s u_e + \beta_3 i_s v_e \\
\frac{dS}{dt} &= \mu_s - k_{-1}e
\end{aligned}\right\} \quad (1.1)$$

Where $e = i_e + u_e$ & $S = i_s + u_s$

In the system (1.1), μ_e is specific growth rate of enzyme, A is the constant amalgamation rate and k_{+1} is forward reaction rate constant. c is the total concentration of the enzyme-substrate complex. γ is the recovery rate of the enzyme concentration and δ is the parameter denotes the air flow rate such that the $v_e$enzyme concentration will join the u_e class. μ_s is specific growth rate of substrate and k_{-1} is its reverse reaction rate. β_2 and β_3 are the interaction rates of operating concentration of substrates with the initial and recovered classes of the enzyme concentration respectively ($\beta 2 > \beta 3$).

The model gives following two cases to be analyzed:

(a) The total concentration of the enzyme-substrate complex c of the operating concentration of enzyme with the infective substrate concentration is a constant, and

(b) It depends upon the initial concentration of substarte. For positive constants $a0$ and $a1$, thus c takes the form

$$c = a_0 + a_1 S.$$

Case (b) is impractical at high concentration such as ours. Therefore, we shall exempt rest of the calculation for this case.

Case a. When $c = c_0;\ c_0$ is a constant

Since $i_e + u_e + v_e = e$ & $i_s + u_s = S$, the system (1.1) can be reduced to the form:

$$\left.\begin{aligned} \frac{du_e}{dt} &= c_0(e - u_e - v_e)u_s - (\gamma + k_{+1})u_e \\ \frac{dv_e}{dt} &= \gamma(u_e) - (k_{+1} + \delta)v_e \\ \frac{de}{dt} &= \mu_e + A - k_{+1}e \\ \frac{du_s}{dt} &= -k_{-1}u_s + \beta_2(S - u_s)u_e + \beta_3(S - u_s)v_e \\ \frac{dS}{dt} &= \mu_s - k_{-1}e \end{aligned}\right\} \quad (1.2)$$

The region of attraction of the above system is

$T_1 = \{(u_e, v_e, e, u_s, S): 0 \le u_e + v_e \le N_1 \le \bar{e}, 0 \le u_s \le S \le \bar{S}\}$,

Where $\bar{e} = \lim_{t\to\infty} \sup e = \frac{\mu_e + A}{k_{+1}}$ & $\bar{S} = \lim_{t\to\infty} \sup S = \frac{\mu_s}{k_{-1}}$.

There exist the following three equilibra corresponding to the system (1.2), namely:

(1) $E_0\left(0,0,\frac{\mu_e+A}{k_{+1}},0,0\right)$.

(2) $E_1\left(0,0,\frac{\mu_e+A}{k_{+1}},0,\frac{\mu_s}{k_{-1}}\right)$ &

(3) $E_2(\overline{u_e},\overline{v_e},\bar{e},\overline{u_s},\bar{S})$, where

$$\overline{u_e}=\frac{c_0\bar{e}\bar{S}\left(\beta_2+\frac{\beta_3\gamma}{k_{+1}+\delta}\right)-k_{-1}(\gamma+k_{+1})}{\left(\beta_2+\frac{\beta_3\gamma}{k_{+1}+\delta}\right)\left\{c_0\left(1+\frac{\gamma}{k_{+1}+\delta}\right)\bar{S}+(k_{+1}+\delta)\right\}},$$

$$\overline{u_s}=\frac{\left(\beta_2+\frac{\beta_3\gamma}{k_{+1}+\delta}\right)\bar{S}\,\overline{u_e}}{\left(\beta_2+\frac{\beta_3\gamma}{k_{+1}+\delta}\right)\bar{Y}_1+k_{-1}}$$

$$\overline{v_e}=\frac{\gamma\overline{u_e}}{\gamma+k_{+1}},\quad \bar{N}_1=\frac{\mu_e+A}{k_{+1}},\bar{N}_2=\frac{\mu_s}{k_{-1}},\quad (1.3)$$

The equilibrium E_2 exists if

$$R_0=\frac{c_0\bar{e}\bar{S}\left(\beta_2+\frac{\beta_3\gamma}{k_{+1}+\delta}\right)}{k_{-1}(\gamma+k_{+1})}>1,\quad (1.4)$$

We state the local stability of the three equilibria E_0, E_1, E_2 in the following theorem.

The equilibrium E_0 is stable. The equilibrium E_1 is stable if $R_0 < 1$, otherwise if $R_0 > 1$, it is unstable and the equilibrium E_2 exists and is stable if $q_1q_2 - q_3 > 0$.

The general variational matrix M corresponding to the system (1.2) is

$$M=\begin{pmatrix}-(c_0u_s+\gamma+k_{+1}) & -c_0u_s & c_0u_s & -c_0(\bar{e}-u_e-v_e) & 0\\ \gamma & -(k_{+1}+\delta) & 0 & 0 & 0\\ 0 & 0 & -k_{+1} & 0 & 0\\ \beta_2(\bar{S}-\bar{u}_s) & \beta_3(\bar{S}-\bar{u}_s) & 0 & -(\beta_2u_e+\beta_3v_e+k_{-1}) & (\beta_2u_e+\beta_3v_e)\\ 0 & 0 & 0 & 0 & -k_{-1}\end{pmatrix}$$

At the Equilibrium point $E_0(0,0,\frac{\mu_e+A}{k_{+1}},0,0)$, the variational matrix M_0

$$M_0=\begin{pmatrix}-(\gamma+k_{+1}) & 0 & 0 & c_0\left(\frac{\mu_e+A}{k_{+1}}\right) & 0\\ \gamma & -(k_{+1}+\delta) & 0 & 0 & 0\\ 0 & 0 & -k_{+1} & 0 & 0\\ 0 & 0 & 0 & -k_{-1} & 0\\ 0 & 0 & 0 & 0 & -k_{-1}\end{pmatrix}$$

The characteristic polynomial corresponding to the above matrix is

$$(k_{+1}+\lambda)(k_{-1}+\lambda)^2(k_{+1}+\delta+\lambda)(k_{+1}+\gamma+\lambda)=0$$

Which gives all the negative roots of λ.

Thus, the equilibrium E_0 is stable.

At the equilibrium point $E_1(0,0,\frac{\mu_e+A}{k_{+1}},0,\frac{\mu_s}{k_{-1}})$, the variational matrix is given by

$$M_1 = \begin{pmatrix} -(\gamma + k_{+1}) & 0 & 0 & c_0\left(\frac{\mu_e + A}{k_{+1}}\right) & 0 \\ \gamma & -(k_{+1} + \delta) & 0 & 0 & 0 \\ 0 & 0 & -k_{+1} & 0 & 0 \\ \frac{\beta_2\mu_s}{k_{-1}} & \frac{\beta_2\mu_s}{k_{-1}} & 0 & -k_{-1} & 0 \\ 0 & 0 & 0 & 0 & -k_{-1} \end{pmatrix}$$

The characteristic polynomial corresponding to the above matrix is given by

$$(k_{+1} + \lambda)(k_{-1} + \lambda)(\lambda^3 + p_1\lambda^2 + p_2\lambda + p_3) = 0 \qquad (1.5)$$

Where

$$p_1 = 2k_{+1} + k_{-1} + \delta + \lambda$$

$$p_2 = -c_0\beta_2\bar{e}\bar{S}\gamma - (\delta + k_{+1})(k_{+1} + \gamma) + k_{-1}(2k_{+1} + \delta + \gamma),$$

$$p_3 = -c_0\beta_3\bar{e}\bar{S}\gamma - c_0\beta_2\bar{e}\bar{S}(k_{+1} + \delta) + k_{-1}(\gamma + k_{+1})(\delta + k_{+1})$$

We find that the eigen values of (1.5) are $-k_{+1}$, $-k_{-1}$ & the roots of the polynomial $\lambda^3 + p_1\lambda^2 + p_2\lambda + p_3$.

The above polynomial has roots with negative real part if $p_1p_2 - p_3 > 0$. Hence,

$$p_1p_2 - p_3 = (\gamma + k_{+1})^2(k_{+1} + \delta) + k_{-1}(2k_{+1} + \delta + \gamma)(k_{+1} + \gamma + k_{-1}) + c_0\beta_3\frac{\mu_s}{k_{-1}}\gamma\left(\frac{\mu_e + A}{k_{+1}}\right)$$

Which is positive. Therefore, the stability of E_1 is given by the sign of p_3, which is positive if and only if $R_0 < 1$. For $R_0 > 1$, E_1 is unstable & E_2 exists.

At the equilibrium point $E_2(\overline{u_e}, \overline{v_e}, \bar{e}, \overline{u_s}, \bar{S})$, the variational matrix M_2 is given by

$$M_2 = \begin{pmatrix} -(c_0\overline{u_s} + \gamma + k_{+1}) & -c_0\overline{u_s} & c_0\overline{u_s} & -c_0(\bar{e} - \overline{u_e} - \overline{v_e}) & 0 \\ \gamma & -(k_{+1} + \delta) & 0 & 0 & 0 \\ 0 & 0 & -k_{+1} & 0 & 0 \\ \beta_2(\bar{S} - \overline{u_s}) & \beta_3(\bar{S} - \overline{u_s}) & 0 & -(\beta_2\overline{u_e} + \beta_3\overline{v_e} + k_{-1}) & (\beta_2\overline{u_e} + \beta_3\overline{v_e}) \\ 0 & 0 & 0 & 0 & -k_{-1} \end{pmatrix}$$

The characteristic polynomial corresponding to the above matrix is

$$(k_{+1} + \lambda)(k_{-1} + \lambda)(\lambda^3 + q_1\lambda^2 + q_2\lambda + q_3) = 0$$

Where,

$$q_1 = \beta_2\overline{u_e} + \beta_3\overline{v_e} + k_{-1} + c_0\overline{u_s} + \gamma + 2k_{+1} + \delta$$

$$q_2 = (d_1 + \delta)(\beta_0\overline{u_s} + \gamma + k_{+1}) + (c_0\overline{u_s} + \gamma + 2k_{+1} + \delta) \times (\beta_2\overline{u_e} + \beta_3\overline{v_e} + k_{-1})$$
$$-c_0\beta_2(\bar{e} - \overline{u_e} - \overline{v_e})(\bar{S} - \overline{u_s}) + c_0\gamma\overline{u_s}$$

$$q_3 = (k_{+1} + \delta)(c_0\overline{u_s} + \gamma + k_{+1})(\beta_2\overline{u_e} + \beta_3\overline{v_e} + k_{-1})$$
$$- \gamma c_0\beta_3(\bar{e} - \overline{u_e} - \overline{v_e})(\bar{S} - \overline{u_s})(k_{+1} + \delta)$$
$$-c_0\beta_2(\bar{e} - \overline{u_e} - \overline{v_e})(\bar{S} - \overline{u_s})(k_{+1} + \delta) + \gamma c_0\overline{u_s}(\beta_2\overline{u_e} + \beta_3\overline{v_e} + k_{-1})$$

$q_1q_2 - q_3 = (\gamma + k_{+1} + c_0\overline{u_s})^2(k_{+1} + k_{-1} + \delta + \beta_2\overline{u_e} + \beta_3\overline{v_e}) + \gamma c_0\beta_3(\bar{e} - \overline{u_e} - \overline{v_e})(\bar{S} - \overline{u_s})$.

It is seen that $q_1q_2 - q_3 > 0$. Hence, the equilibrium point E_2 is locally asymptotically stable. The system (1.2) is then integrated using the fourth-order Runge-Kutta method [28]. The physical significance of this set of equations is tested experimentally, where detailed discussion is shown in section for stack reversal operation of BSMFC.

5.Performance Analysis

Polarization curves were generated using continuous flow of feedstock into the MFCs at constant flow rates to give anodic chamber dilution rates of $0.04h^{-1}$. The BSMFC produced an open-circuit potential of 1.60 V with an acidified catholyte. Changing the recirculation of the anolyte did not significantly affect the power output in a short period, but a long-term test demonstrated improved electricity production at higher recirculation rates. Lowering the pH of the catholyte benefited the cathode reaction and increased power production; however, pH is not the only factor affecting the cathode reaction, voltage reversal (discussed in later section) also decreased electricity generation.

Under these operation conditions, the COD removal rate was 1.2 mg/L min (58% COD removal). The maximum power density at a flow rate of 0.22 mL/min, obtained by varying the circuit resistance from 50 to 290 Ω, was 6.9 W/m^3 with a current of 4 mA (100 Ω). This power density is about 10% higher than that obtained under typical operating conditions with a 470 Ω resistor. Increasing the HRT to 5.0 h decreased the power density to 6($1W/m^3$) and the COD removal rate to 1.0 mg/L min (79% removal; influent COD) 280 (19 mg/L; log mean COD) 141 mg/L; data not shown). When the HRT was decreased to 1.1 h (0.39 mL/min), the average power generation was 72 (1 W/m^3 with a COD removal rate of 2.4 mg/L min (42% removal; influent COD) 379 (9

mg/L; log mean COD) 292 mg/L). This power density was 2.8 times larger than that obtained in previous tests using wastewater. Power density showed a Monod-type trend as a function of the wastewater strength over a range of 38- 324 mg COD/L.

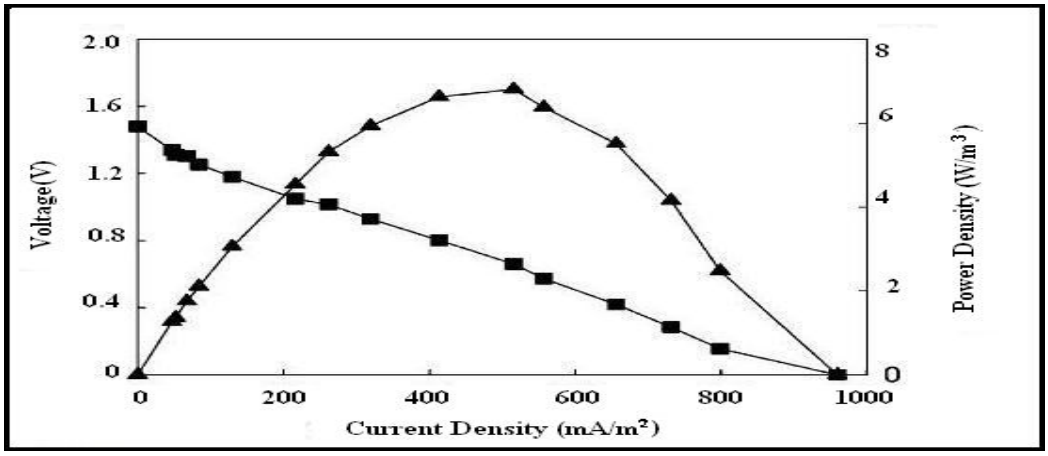

Figure1: Polarization curve for BSMFC. Voltage (■) & power density (▲).

5.Fuzzy Logic Energy Harvester For BSMFC

Fig.1. shows the structure of the closed-loop fuzzy control system. A fuzzy control system with dual inputs is used to control the output power of the fuel cell, where P_{fc}^{*} is the set point value of the output power. The error *e*(*k*), the change in error *ec*(*k*) and the control output *u*(*k*) of the fuzzy controller are given as：

$$e(k) = P_{fc}^{*} - P_{fc} \quad (2)$$

$$ec(k) = e(k) - e(k-1) \quad (3)$$

$$u(k) = u(k-1) + \Delta u(k) \quad (4)$$

Here $\Delta u(k)$ is the inferred change of duty ratio by fuzzy controller. The triangular type membership function is chosen for error, change of error, and output control variable. The fuzzy domain for *e*, *ec* is [-1, 1], and for *u* is [1, 10]. The fuzzy set for *e* is {NB, NS, ZE, PS, PB}, and for *ec* and *u* is {NB, NM, NS, ZE, PS, PM, PB}. The membership functions for input error *e*, change of error *ec* and output control *u* are shown in Fig.5 to Fig.7.

The output control *u* of the fuzzy controller is designed as its dependency on the input molar flow of oxygen of the fuel cell.

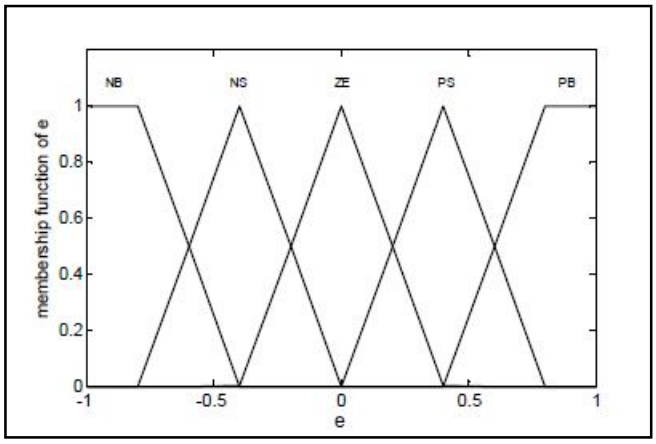

Figure 5:Membership function of the error e

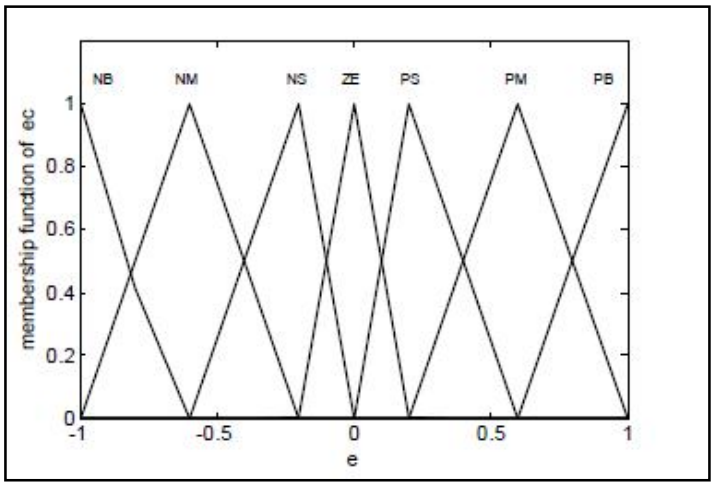

Figure 6: Membership function of the change of error ec

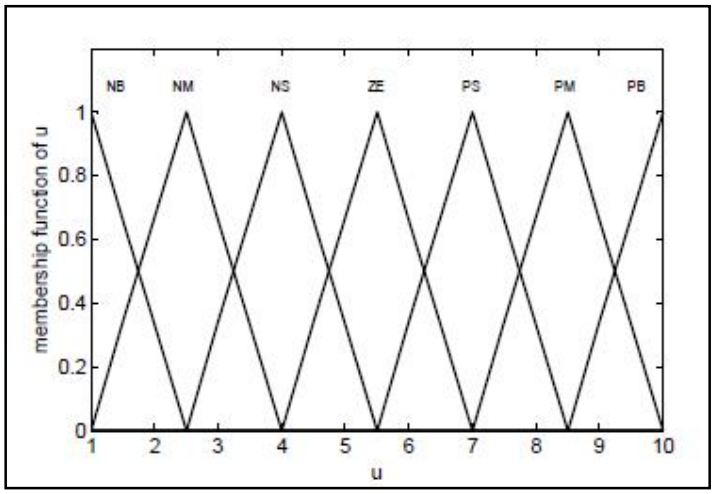

Figure 7: Membership function of the control u

u		*e*				
		NB	NS	ZE	PS	PB
ec	NB	ZE	ZE	NB	ZE	ZE
	NM	ZE	ZE	NM	ZE	ZE
	NS	ZE	ZE	NS	ZE	ZE
	ZE	NB	NS	ZE	PS	PB
	PS	ZE	ZE	PS	ZE	ZE
	PM	ZE	ZE	PM	ZE	ZE
	PB	ZE	ZE	PB	ZE	ZE

Table 1:Fuzzy control rules

The system operating voltage has been determined from the polarization curve. The proposed fuzzy controller keeps the harvesting system operating in the vicinity of the maximum power point of the MFC. This control scheme changes the power extraction frequency according to the MFC's condition to maintain the MFC voltage at a pre-defined range and ensures enough recovery time of the MFC reactor. This scheme is effective especially when the MFC internal voltage drops significantly as output current increases. The layer facilitates the output voltage to an appropriate level for powering the external electronic device(s).

The operation of the energy harvester in the first layer consists of two modes, CHARGE and DISCHARGE, according to the energy flow on the inductor connected with the MFC. During the CHARGE mode, the harvesting converter's MOSFET *Q* is on, and the energy is extracted from the MFC and stored in the inductor *L*. The MFC terminal voltage in this mode decreases due to the increasing current. Assuming negligible inductor resistance and constant internal voltageV_{int}, the instantaneous MFC output voltage and current in a CHARGE period can be given as follows, where I_{oc} is the initial inductor current when MOSFET *Q* is closed.

$$i(t) = \frac{1}{L_1}\int \left(V_{int} - R_{int} i(t)\right)dt \quad (5)$$

$$= \left(I_{oc} - \frac{V_{int}}{R_{int}}\right) e^{\frac{-R_{int}}{L1}t} + \frac{V_{int}}{R_{int}} \quad (6)$$

$$V_{MFC}(t) = V_{int} - R_{int} i(t) \quad (7)$$

It can be seen that the current would be increasing to a level determined by the internal voltage and the resistance, which is the overall maximum current in the polarization curve. However, the energy harvesting controller keeps the current at the level of the

maximum power operating point. The external inductance and the internal resistance determine the changing rate of voltage and current, which determines the energy extracting frequency as well. During the DISCHARGE mode, the MOSFET switch *Q* is off, and the energy stored in the inductor *L* is discharged to the storage capacitor *C*. The MFC voltage increases in this mode as current decreases. The MFC output current and the storage capacitor voltage in the DISCHARGE mode can be given as follows.

$$i(t) = \frac{1}{L}\int (V_{int} - R_{int} i(t) - V_{01})dt \quad (8)$$

$$= \left(I_{od} - \frac{V_{int} - V_{01}}{R_{int}}\right) e^{\frac{-R_{int}}{L1}t} + \frac{V_{int} - V_{01}}{R_{int}} \quad (9)$$

Where, $$V_{01}(t) = \frac{1}{C}\int (i(t) - I_L)dt \quad (10)$$

I_{od} and I_L is the inductor current when MOSFET *Q* is open and the load current drawn from the

storage capacitor *C*, respectively. The instantaneous current is a function of internal voltage, internal resistance, external inductance, external capacitance, and load current in DISCHARGE mode.

For an efficient BSMFC energy harvester using DC converters the given circuital scheme has been implemented. This energy harvester captures the energy from BSMFCs in the moderately efficient operating point and at the same time forms the energy into a usable shape. Furthermore, parallel operation using multiple BSMFCs is straightforward. Optimal operating conditions and converter parameters, and real-time operating point tracking for the control scheme for more robust and efficient operations of BSMFCs. It cuts the activation loss as in order to start the transfer of electrons from the electrochemical active microorganisms towards the electrode or to transfer electrodes towards a final electron acceptor, an energy barrier must be overcome, leaching to voltage loss or activation over potential characterized by initial steep decrease of cell voltage at the onset of electricity generation. Activation losses can be reduced by increasing electrode surface area, improving electrode catalysts, increasing operating temperature slightly (as microbes may die) and the establishment of enriched bio-film on the electrode.

6.Limitation Of BSMFC: Voltage Reversal In MFC Stacks

When operated in continuous flow mode, the system produced continuous power and all cell voltages remained positive. The stack voltage ranged from 0.8 to 0.9V when the stack is fed adequate acetate (0.1 M) at a hydraulic retention time of 3 h in each cells (external load of 500Ω). When the system is operated in fed-batch mode, positive cell voltages was maintained in both cells only at the beginning of each cycle. At an external load of 30Ω, for example, the voltages at the beginning of the cycle were 1.6 V. At the end of every batch cycle, however, it was observed that the voltage in adjacent cells was reversed. After 5 h of operation, for example, the voltage of Cell I was 0.6V while the voltage in Cell II decreased to −0.6V. Voltage reversal is well known to occur in hydrogen fuel cells when one of the cells suffers loss of the fuel or exhibits a much larger resistance than other cells in the stack. We therefore examined whether voltage reversal will be due to differences in substrate concentrations in two cells, as shown above in the electrochemical modeling.

The exact measurement of electrochemical model (discussed above in modeling section) is quiet complex. Therefore, we have divided our experiment in two parts. First, we try to prove that substrate concentration can affect voltage generation. Voltage output by the two adjacent cell stack is relatively stable at 0.5V at an acetate concentration of >12 mM, but the voltage decreased in proportion to substrate concentration at lower acetate concentrations. This effect of substrate concentration on voltage is consistent with that previously observed with a single-cell MFC.

Second, we demonstrated that low substrate concentration would produce voltage reversal by intentionally starving one of the adjacent cells over a cycle by not feeding it substrate. As depicted in the first cycle when both cells were fed substrate (acetate), positive voltages were initially produced in the two cells at the beginning of the cycle producing a total stack voltage of 0.38V. However, the voltage in Cell I was lower than that of Cell II at the beginning of this first cycle. Thus, after this initial period Cell I demonstrated voltage reversal with Cell II having a positive voltage throughout the first cycle. Thus, the weaker cell at the beginning of the cycle is the one that will undergo voltage reversal (also supported by the previous results). We next demonstrated that we could make adjacent cell undergo charge reversal by not feeding it (i.e., having it produce less voltage than other). In the second cycle, we starved few cells (no substrate), making it the weaker cell compared to the leftover cell, and thus, leftover cells showed voltage reversal. The maximum stack voltage for this second cycle was now only 0.06V.

Third, we fed both cells again to see which cell would undergo charge reversal. In this third cycle, we observed that Cell Iinitially produced less voltage than Cell I, and that it then showed charge reversal. By starving Cell II over a whole feeding cycle we made it the weaker cell in the third cycle, and we produced voltage reversal in it even though both cells were fed the same amount of substrate. This shows that prolonged starvation adversely affected Cell II, making it the weaker cell, and that the weaker cell will be the one to undergo charge reversal.

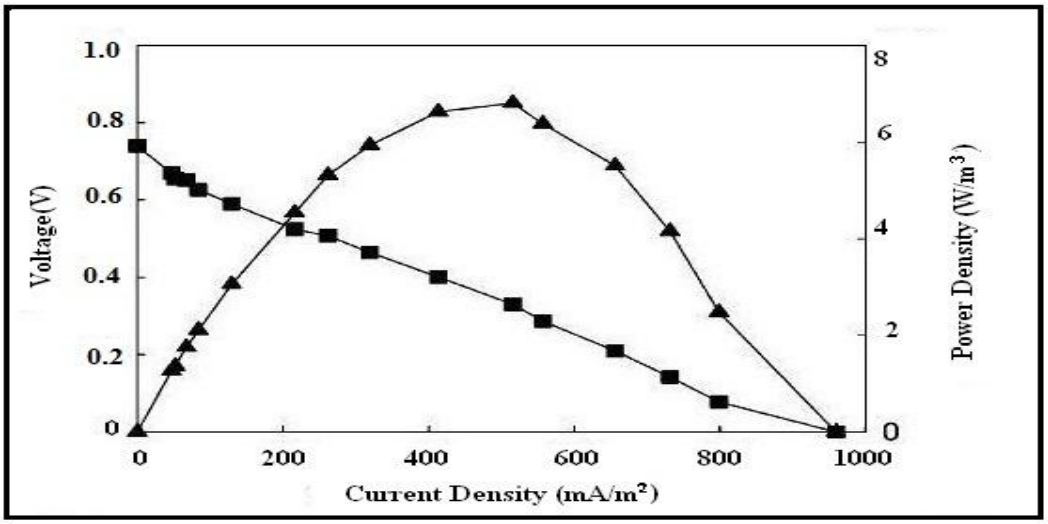

Figure8. Change of voltage after voltage reversal

The output voltage V_{fc} of a single cell can be defined as the result of the following expression：

$$V_{fc} = E_{nerst} - V_{act} - V_{ohmic} - V_{rev} \quad (11)$$

in which E_{nerst} is the thermodynamic potential of the cell representing its reversible voltage, and

$$E_{nerst} = 1.229 - 0.85 \times 10^{-3}(T_{fc} - 298.15) + 4.31 \times 10^{-5} T_{fc} \left[\ln(P_{H_2}) - \frac{1}{2}\ln(P_{O_2})\right] \quad (12)$$

Where P_{H_2} and P_{O_2} are the pressure of hydrogen and oxygen respectively, and T_{fc} is the operating temperature. The voltage drop due to the activation of the anode and the cathode is given byV_{act} as:

$$V_{act} = 0.9514 - 3.12 \times 10^{-3} T_{fc} - 7.4 \times 10^{-5} T_{fc} \ln(C_{O_2}) + 1.87 \times 10^{-4} T_{fc} \ln(i) \quad (13)$$

$$V_{ohmic} = i(R_C + R_m) \quad (14)$$

where i is the electrical current, and C_{O_2} is the oxygen concentration. V_{ohmic} is the ohmic voltage drop associated with the conduction of cations through the electrolyte, and anions through the internal electronic resistance.

V_{ewv} is the reversal voltage drop resulting(as noticed during the experiment) from the mass transportation effects, which affects the concentration of the reacting gases and can be described by the following expression:

$$V_{rev} = -R_o \ln\left(1 - \frac{i}{i_{max}}\right) \quad (15)$$

Here, value of R_o is determined from equation (1.4), i_{max} is the maximum electrical current of the fuel cell.

7.Conclusion

The novelty of the present study lies in the demonstration of more efficient microbial-power harvesting system that could produce higher energy density levels. Additionally, to enquire about the potential power losses. As inferred in this study, the perspective of sustainable maximum power transfer is achieved using parallel stacked arrangement of brush anode with series cathode chamber. The Next aim of this study is in energizing real-world applications of MFCs to deliver maximum power of 1.6 V across the load. It has been found that the power density is not maintained at the same level during the whole experimental operation. Except for the first phase of the experiment, we failed to generate continuous high power when MFCs are enlarged. In addition with that we addressed few issues regarding power losses that were unknown earlier, at this reactor scale. With a plurality of bulk units, series connection can be used to step up voltage above the level 1.6 V. However, the advantages of further scale-up and plurality have yet to be studied.

Power output, one of the most important features of MFC development, our study a scores few engineering methodology to improve with mL-scale MFCs to Liter scale but a huge wholesome of work is yet to be entertained. In terms of energy recovery, a power density of 150–200 W /m^3, if achieved for longer duration, will make the MFC

technology competitive with conventional anaerobic digesters. To advance MFC technology toward practical application, larger reactors at liter scale (L-scale) must be constructed and investigated.

8.Reference

1. Potter M.C., 1911, Electrical effects accompanying the decomposition of organic compounds, Proc. R. Soc. Lond. B. Biol. Sci. Vol. 84, 260–276.
2. Min, B., Cheng, S. and Logan B. E. (2005). Electricity generation using membrane and salt bridge microbial fuel cells, Water Research, 39 (9), pp1675–86
3. Cohen, B. (1931). The Bacterial Culture as an Electrical Half-Cell, Journal of Bacteriology, 21, pp18–19
4. DelDuca, M. G., Friscoe, J. M. and Zurilla, R. W. (1963). Developments in Industrial Microbiology. American Institute of Biological Sciences, 4, pp81–84.
5. Karube, I., T. Matasunga, S. Suzuki & S. Tsuru. (1976). Continuous hydrogen production by immobilized whole cells of Clostridium butyricum Biocheimica et Biophysica Acta 24:2 338–343
6. Karube, Isao; Matsunaga, Tadashi; Tsuru, Shinya; Suzuki, Shuichi (November 1977). "Biochemical cells utilizing immobilized cells ofClostridium butyricum". Biotechnology and Bioengineering 19 (11).
7. Allen, R.M.; Bennetto, H.P. (1993). "Microbial fuel cells: Electricity production from carbohydrates".Applied Biochemistry and Biotechnology 39-40: 27–40.
8. Delaney, G. M.; Bennetto, H. P.; Mason, J. R.; Roller, S. D.; Stirling, J. L.; Thurston, C. F. (2008). "Electron-transfer coupling in microbial fuel cells. 2. Performance of fuel cells containing selected microorganism-mediator-substrate combinations". Journal of Chemical Technology and Biotechnology. Biotechnology 34: 13.
9. Lithgow, A.M., Romero, L., Sanchez, I.C., Souto, F.A., and Vega, C.A. (1986). Interception of electron-transport chain in bacteria with hydrophilic redox mediators. J. Chem. Research,(S):178–179.
10. A.K. Manohar, F. Mansfeld, Electrochim. Acta 54 (2009) 1664.
11. Suman Sahai. 1999, Biotechnology capacity of LDCS in the Asian Pacific Rim. AgBioForum – Volume 2, Number 3 & 4 – Pages 189-197.
12. Atlas, R.M., 1992, Molecular methods for environmental monitoring & containment of genetically engineered microorganisms. Biodegradation 3, 137-146.
13. Logan B. (May 2009). "Exoelectrogenic bacteria that power microbial fuel cells". Nature Reviews Microbiology 7: 375–383.

14. Hartshorne R., et al. (Dec 2009). "Characterization of an electron conduit between bacteria and the extracellular environment".Proceedings of the National Academy of Sciences 106: 22169–22174.
15. Zhang, Fei (2010) Effects of anolyte recirculation rates and catholytes on electricity generation in a litre-scale upflow microbial fuel cell. Energy & Environmental Science, 2010, 3, 1347–1352.
16. Peter Clauwaert, Schalla Mulenga, Peter Aelterman and Willy Verstraete, 2009, Litre-scale microbial fuel cells operated in a complete loop. APPLIED MICROBIOLOGY AND BIOTECHNOLOGY Volume 83, Number 2 (2009), 241-247, DOI: 10.1007/s00253-009-1876-0.
17. Rabaey, K. et al. (2004) Biofuel cells select for microbial consortia that self-mediate electron transfer. Appl. Environ. Microbiol. 70, 5373–5382.
18. Liu, H. and Logan, B.E. (2004) Electricity generation using an aircathode single chamber microbial fuel cell in the presence and absence of a proton exchange membrane. Environ. Sci. Technol. 38, 4040–4046.
19. Larminie, J. and Dicks, A. (2000) Fuel cell systems explained, John Wiley & Sons.
20. Gil, G.C. et al. (2003) Operational parameters affecting the performance of a mediator- less microbial fuel cell. Biosens. Bioelectron. 18,327–334.
21. Liu, H.; Ramnarayanan, R.; Logan, B. E., 2004, Production of electricity during wastewater treatment using a single chamber microbial fuel cell. Environ. Sci. Technol., 38, 2281-2285.
22. Zuo, Y., Cheng, S., Call, D., Logan, B.E., 2007. Tubular membrane cathodes for scalable power generation in microbial fuel cells. Environ. Sci. Technol. 41, 3347–3353.
23. You, S.J., N.Q. Ren, Q.L. Zhao, J.Y. Wang and F.L. Yang, 2009. Power generation and electrochemical analysis of biocathode microbial fuel cell using graphite fibre brush as cathode material. Fuel Cells, 9: 588-596.
24. Clauwert, P., Aelterman, P., Pharm, H.T., DeSchamphelaire, L., Carballa, M., Rabaey, K. And Verstraete, W. (2008). Minimizing losses in bio-electrochemical systems: the road to application. Application of Microbial biotechnology Vol. 79 p 901